Toppling of Rigid Electric Equipment during Earthquakes

Miguel A Jaimes,[a)] and Gabriel Candia[b)]

ABSTRACT

This study presents a general formulation for toppling risk assessment of rigid electrical equipment during earthquakes. The seismic response, toppling fragility functions and toppling risk were examined for three types of support conditions, namely: 1) equipment simply supported on the foundation; 2) equipment anchored to the foundation; and 3) equipment supported on a seismic base isolator. Because empirical fragility functions for overturning equipment remain insufficient, the present study relies on numerical analysis and a solid physical background to compute risk. These results should aid designers in the selection of appropriate support conditions or mitigation measures for rigid electric equipment in seismic prone regions.

As an example, the toppling risk methodology is presented using Mexican seismicity and a set of nine electrical equipment commonly used throughout Mexican power stations, with heights between 3 and 5 m, covering an ample range of frequency parameters ($1.54 < p < 2.16$ rad/s), and block dimensions ($1.58 \text{ m} < R < 2.49$ m). Further, the effects of site-to-source distance for sites located on firm soil are studied in detail, as the frequency content of these ground motions differ significantly and play a key role in the toppling vulnerability of the blocks. The study shows that the reliability index increases monotonically with increasing block aspect ratio and block size for the nine equipment and the three support conditions studied. This investigation also demonstrates that the reliability of free-standing equipment due to near-source ground motions is slightly higher than that of anchored equipment or base isolated equipment. In contrast, for far-field ground motions, the reliability for anchored equipment is slightly higher than that of free-standing or base isolated equipment.

KEYWORDS Toppling Risk, Rigid Electric Equipment

a) Instituto de Ingeniería, UNAM, Av. Universidad, No. 3000, CP 04510, Del. Coyoacán, México D.F. E-mail: mjaimest@iingen.unam.mx

b) Facultad de Ingeniería, Universidad del Desarrollo, Av. Plaza 680 Las Condes, Santiago – Chile. National Research Center for Integrated Natural Disaster Management CONICYT/FONDAP/15110017.

1. INTRODUCTION

Recent seismic events show that electrical power plants are highly vulnerable to service disruption resulting from overturned or collapsed equipment such as transformers, control stations, and other heavy equipment (Figure 1). Case studies of power plant failures during earthquakes (e.g., [1-3]) show that the collapse of electrical equipment causes not only direct economic losses due to the repair/replacement costs of damaged equipment, but also indirect socio-economic impacts as a consequence of power outage. For instance, the collapse of circuit breakers and transformers during the 1999 Izmit earthquake, Turkey [3] led to direct loses of $70 million and power disruption over a vast region. Likewise, severe damage on numerous 500 kV switchyards during the 1989 Loma Prieta earthquake, U.S. [1] caused direct loses of $4.9 million.

(a)  (b) 

Fig. 1. (a) Collapse of anchored electrical equipment during the 1971 Mw 6.6 San Fernando Earthquake [4], and (b) toppled transformer during the 1999 Mw 7.4 Izmit earthquake, Turkey[5].

During the Mw 8.0 1995 Colima-Jalisco earthquake in Mexico, the Manzanillo Power Plants 1 and 2 were severely shaken [2]. The most critical damage was observed at the Plant 1 switchyard, where several ceramic columns that support the disconnect switches collapsed, and 9 out of 22 circuit breakers had to be replaced or repaired. Other damage to Plant 1 included the overturning of three potential transformers, leaning and cracking of ceramic columns, disconnected conductors, and leaks of insulating fluids in several transformers. However, none of the transformers had to be replaced, and repairs were inexpensive. At the Manzanillo Plant 2, the ceramic columns of two potential transformers collapsed, and the columns of several disconnect switches were fractured. Approximately 20% of the transformers needed replacement of their ceramic base seals. Direct economic loses from this earthquake were estimated in US$93.5 million [6], of which approximately 11% corresponds to direct losses in the electric power supply; which was interrupted for more than 20 hours, affecting 243,000 people. The restitution of the energy supply was achieved within 72 hours, which is the maximum acceptable recovery time accepted by the international community [7].

More recently, on September 7th, 2017, a Mw 8.2 intermediate-depth normal earthquake struck the Gulf of Tehuantepec in Chiapas, Mexico. It is the largest earthquake in Mexico since the Mw 8.2 Jalisco earthquake of 1932. According to preliminary reconnaissance information, the earthquake caused severe damage at near-source locations, such as houses, historical and world heritage buildings, bridges, electrical substations, and equipment. No damage was observed on the wind farms located in Oaxaca (approximately 1,186 wind turbines), but the Mw 8.2 earthquake damaged electrical substations and 21 wind farms in the Istmo region had to shut down; all electrical substations suffered damage of circuit breakers and transformers [8]. The wind farms restarted operation at near 80% capacity almost 70 days after the earthquake.

Similarly, no structural damage was reported at the state-owned Salina Cruz Refinery, the largest refinery in Mexico with an installed capacity of 330,000 barrels per day. The earthquake, however, induced lateral displacements on the 70 MW electrical generators that power the plant [9]. As a result, the plant was shut down as a precaution and operations were resumed almost 2.5 months later. For more details about damage reported in substations during other previous earthquakes, refer to [10].

Guaranteeing the service continuity of power stations at all times is critical; particularly, after severe natural disasters all components should continue operating to support the emergency response efforts and the needs of the population. Thus, the toppling of electrical equipment during earthquakes and the consequences of power outages, has prompted research on the dynamic response of rigid bodies and the design of collapse mitigation measures. Importantly, current seismic design standards (e.g., [11-13]) provide recommendations for evaluating the overturning of equipment, generally in the form of pseudo-static analyses, but do not define collapse performance objectives explicitly, such as the limit of 1% probability of collapse in 50 years recommended by ASCE7-10 [14] for structural components.

Modelling the rocking response of rigid blocks is extremely cumbersome, yet predictable in a statistical sense [15]. Still, one of the main challenges is to properly account for energy dissipation and the chaotic nature of the block response modes (e.g., rocking, sliding, uplifting, free flight) [16]. Nevertheless, simplified or idealized models have proved successful to understand the block dynamics due to real earthquakes and have guided the engineering practice in the last 50 years.

The response of free-standing rigid blocks to a base excitation is founded on the principles of rigid body dynamics, for which a vast body of literature exists, e.g., [15-30]. After examining the response of inverted-pendulum structures in the 1960 Valdivia earthquake (Chile), Housner [17] studied the reliability of slender blocks under simple sinusoidal base motions and the effects of block scale in the stability, and demonstrated that given two geometrically similar blocks, the larger one is more stable. Later, Yim et al., (1980) [18] developed probabilistic estimates of the rocking response of rigid blocks, and Psycharis and Jennings (1983) [19] analyzed the problem of rigid and semi-rigid blocks supported on a flexible foundation, in which uplift was allowed and horizontal slip was restrained. A study about the response of electrical equipment subjected to near-source ground motions [20] concluded that although both large and small blocks are sensitive to long-duration pulses, the toppling of small blocks is more sensitive to acceleration pulses of short-duration (high frequency), whereas larger blocks need a larger duration pulse to overturn. More recently [21], closed form solutions were developed for a free-standing rectangular block subjected to generalized half-cycle pulses using linearized equations of motion. This study revealed complex behavior patterns and provides a simple expression to distinguish safe from overturning block response. The work by Cimellaro et al., (2014) [22], proposed a simplified formula that relates overturning ratios and the ground motion intensity, using a physical model and real earthquake records. Arredondo et al. (2017) [22] studied the response of irregular free standing blocks using a simplified numerical model validated against shaking table results.

Seismic protection measures against block overturning have been studied numerically and experimentally. However, their performance during actual earthquakes has not been thoroughly documented. The most common mitigation measures include the use seismically isolated bases [24-27] and the use of restrainers such as bolts, cables or rubber bands [28-30]. For instance, Caliò and Marletta (2003) [24] developed behavioral maps for symmetric rigid blocks supported on a sliding pedestal connected to a spring-dashpot device, and Contento and

Di Egidio (2009) [26] extended this work to non-symmetric bodies. Later Vassiliou and Makris (2012) [27], developed equations of motion for symmetric blocks considering three types of base isolation hysteresis: linear visco-elastic, bilinear, and trilinear. The authors developed a closed form equation for the maximum coefficient of restitution for a block standing on an isolated base and concluded that base isolation is more effective in relatively small blocks. The study also concluded that large blocks subjected to moderate period pulses are significantly more stable when they rest free on a fixed base compared to an isolated base, even for very flexible isolation interfaces.

Although very attractive as a mitigation measure, the study of anchored blocks has received much less attention in the literature. Available studies include the use of elasto-brittle or elasto-plastic anchors for rigid blocks supported on a fixed base [28, 29], and blocks anchored to a rocking base [30]. These studies show that restrainers are more efficient in preventing overturning of small slender blocks, and that for certain ground motions, the restrainers can have a detrimental effect on the seismic response of the block compared to the block without restrainers. The model details of the base isolated equipment and anchored equipment are discussed in the next section.

The purpose of the present study is to evaluate the seismic toppling risk of rigid rectangular blocks, such as transformers, power generators, or control cabinets, based on numerical solutions of the governing differential equations and the site-specific seismic hazard. Three different equipment configurations are considered in the analysis: 1) equipment simply supported on a fixed base; 2) equipment fixed to a base with ductile anchors; and 3) equipment simply supported on an isolated base. The formulation is applicable to any seismic region and type of overturning equipment. As an example, this study uses the Mexican seismicity and Mexican electrical equipment to illustrate the effect of near-source and far-field ground motions on the collapse fragility functions and reliability indices. Design recommendations are provided for the type of overturning mitigation measure appropriate for these different seismic environments. Finally, this study provides reference values of the toppling risk for typical electrical equipment subject to ground motions with different frequency content (i.e., near-source versus far-field ground motions), which are mainly a function of the block's aspect ratio.

2. METHODOLOGY

The computation of the toppling risk of electrical equipment consists of three basic steps: (i) evaluation of the seismic response; (ii) development of fragility functions; and (iii) convolution of seismic hazard and fragility functions. These steps are briefly explained next.

2.1 SEISMIC RESPONSE OF ELECTRICAL EQUIPMENT

Three equipment configurations are considered in this study: (i) equipment simply supported on a fixed base; (ii) equipment anchored to a fixed base; and (iii) equipment simply supported on seismically isolated base (Figure 2). In all three cases, the ground motion acts along the horizontal axis, the friction between the equipment and the base is sufficiently large to prevent sliding, and the block is not allowed to completely detach from the ground. The mathematical formulation for each model is presented herein.

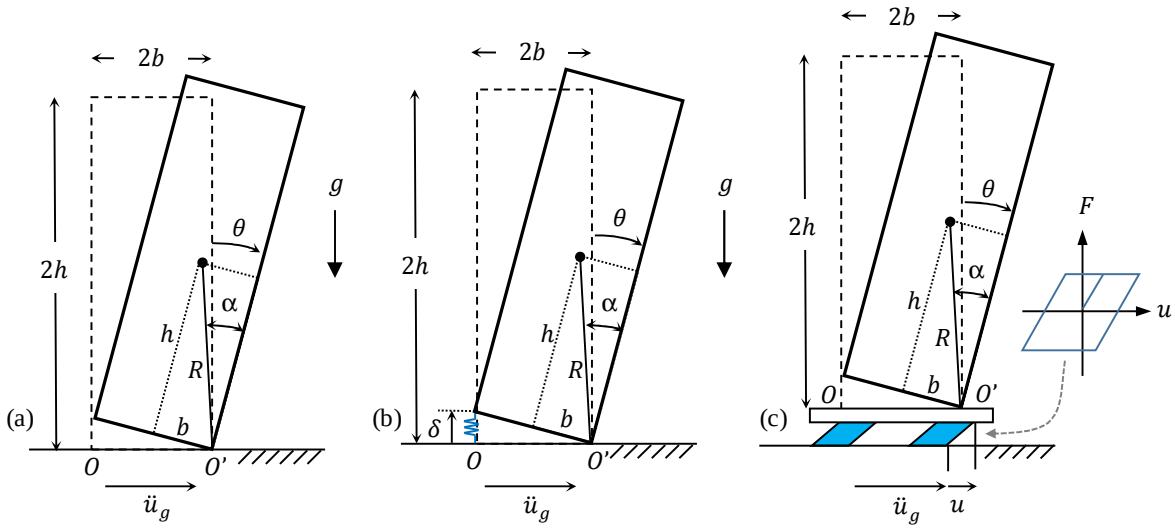

Fig. 2. Schematic view of rigid electrical equipment in rocking motion: a) equipment simply supported on a fixed base; b) equipment anchored to a fixed base; and c) equipment simply supported on a seismically isolated base

2.1.1 Equipment simply supported on a fixed base

The rocking motion of a freestanding rigid block, Figure 2(a), can be modeled as a one degree-of-freedom system. The governing differential equation given by [17]

$$\ddot{\theta}(t) = -p^2\left\{\sin A(t) + \frac{\ddot{u}_g}{g}\cos A(t)\right\} \tag{1.1}$$

where $\ddot{\theta}$ is the angular acceleration of the block, $p = \sqrt{3g/4R}$ is the frequency parameter of the block, $\ddot{u}_g$ is the input ground acceleration, $A(t) = \alpha\ \text{sign}[\theta(t)] - \theta(t)$, R is the block semi diagonal, and $\alpha = \tan^{-1} b/h$ is the block angle. For slender blocks and within the limits of small rotations (i.e., small $A(t)$ values), Eq. (1) can be linearized as shown in Equation (1.2), which can be solved analytically.

$$\ddot{\theta}(t) = -p^2\left\{A(t) + \frac{\ddot{u}_g}{g}\right\} \tag{1.2}$$

When rocking motion occurs, the block impacts the base and the contact points alternate between O and O', Figure 2(a); after each impact, kinetic energy dissipates at a ratio $r = \dot{\theta}_2^2/\dot{\theta}_1^2$, where $\dot{\theta}_1$ and $\dot{\theta}_2$ are the angular velocities immediately before and after the impact. Assuming conservation of angular momentum [17], the maximum theoretical value of r is given by

$$r = \left[1 - \tfrac{3}{2}\sin^2\alpha\right]^2 \tag{2}$$

which is a function of block angle α. Other sources of energy dissipation lead to smaller r values.

2.1.2 Equipment anchored to a fixed base

The seismic response of anchored equipment, Figure 2(b), was based on the formulation presented by Makris and Black (2002) [30]. In this model, anchors are modeled as elasto-

plastic elements with ultimate strength F_u, yield deformation δ_y, ductility capacity ratio μ, and zero post-yield stiffness. The governing set of equations for the anchored equipment is given by

$$\ddot{\theta}(t) = -p^2 \left\{ \sin A(t) + \frac{\ddot{u}_g}{g} \cos A(t) + \frac{3F_u \sin^2 \alpha}{m\delta_y p^2} \theta_y Z(t) \cos\left(\frac{\theta}{2}\right) f(\theta) \right\} \tag{3.1}$$

$$\theta_y \dot{Z}(t) + \zeta \left|\dot{\theta}(t)\right| Z(t) |Z(t)|^{n-1} + \beta \dot{\theta}(t) |Z(t)|^n - \dot{\theta}(t) = 0 \tag{3.2}$$

where $\theta_y = \delta_y / 2b$ is the yield rotation of the restrainer, and $K = F_u/\delta_y$ its pre-yielding stiffness. The hysteretic parameter Z accounts for the non-linear behavior of the restrainers, and the shape of the hysteretic loop is given by a Bouc-Wen model of parameters β, ζ, and n [31, 32]. To account for rupture of the restrainers, a fracture function $f(\theta)$ is introduced in Eq. (3.1), such that

$$f(\theta) = \begin{cases} 1 & if \quad |\theta(t)| < \mu\theta_y \\ 0 & if \quad |\theta(t)| \geq \mu\theta_y \end{cases} \tag{4}$$

Thus, if a restrainer fails, i.e., $f(\theta) = 0$, the equation of motion is reduced to that of a block simply supported on a fixed base. Assuming conservation of angular momentum, the coefficient of restitution r for the anchored block is also given by Eq. (2).

2.1.3 Equipment simply supported on a seismically isolated base

The base isolation solution implemented in this study follows the bilinear model by Vassiliou and Makris (2012) [27], which approximates the hysteresis loops of Single Concave Spherical Sliding (SCSS) systems. Thus, the equation of motion for a block of mass m, supported on a SCSS base of mass m_b, yield displacement u_y, post-yield lateral stiffness k_b, and friction coefficient υ is given by

$$\ddot{\theta}(t) = -p^2 \left(\sin A(t) + \cos A(t) \frac{-\omega_b^2 u(t) - \upsilon g z(t) - \gamma R \left(\dot{\theta}(t)\right)^2 \sin A(t) + \gamma R \cos A(t) p^2 \sin A(t)}{g - \gamma R p^2 \cos^2 A(t)} \right) \tag{5.1}$$

$$\ddot{u}(t) = \frac{-\omega_b^2 u(t) - \upsilon g z(t) - \gamma R \left(\dot{\theta}(t)\right)^2 \sin A(t) + \gamma R \cos A(t) p^2 \sin A(t)}{1 - \frac{\gamma R p^2 \cos^2 A(t)}{g}} - \ddot{u}_g(t) \tag{5.2}$$

$$\dot{z}(t) = \frac{1}{u_y} (\dot{u}(t) - \zeta |\dot{u}(t)| z(t) |z(t)|^{n-1} - \beta \dot{u}(t) |z(t)|^n) \tag{5.3}$$

where $\ddot{u}$ is the acceleration of the isolated base relative to the ground, $\gamma = m/(m_b + m)$, $\omega_b = \sqrt{k_b/(m_b + m)}$, and the dimensionless parameter $z(t)$ is a Bouc-Wen model that describes the non-linear hysteresis of the isolator. Analogous to the fixed base and anchored models, the block rotations on top of the isolated base are continuous from the point O to O', Figure 2(c), and the maximum theoretical energy loss ratio is given by Eq. (6) [25, 27].

$$r = \left[\frac{(\gamma + 4)\cot^2 \alpha - 2(\gamma + 1)}{(\gamma + 4)\cot^2 \alpha + 4(\gamma + 1)} \right]^2 \tag{6}$$

2.1.4 Numerical integration and stopping criterion

Equations (1), (3), and (5) were integrated numerically in conjunction with the theoretical factor r. These equations were written in state format, and solved using an explicit 4th order Runge Kutta method [33] and a time integration step of $\Delta t = 10^{-4}s$. Integration was carried over the entire length of the ground motion, or until the block toppled, i.e. $|\theta(t)| \geq \pi/2$, which is regarded as failure of the electrical equipment.

2.1.5 Validation examples

To verify the fidelity of the solution to Equations (1), (3) and (5), three examples available in the literature were reproduced herein. The response of a simply supported block to a half-sine pulse of duration 0.5 s and angular frequency $\omega_p = 2\pi$ was computed for two limiting cases of maximum ground acceleration using the linear formulation (Figure 3), resulting in excellent agreement with the analytical solution reported by Makris and Roussos 1998 (refer to Figure 2 in [20]). Likewise, the response of simply supported and base isolated blocks to the Jensen Filter Plant motion, shown in Figure 4, successfully matched the results by Vassiliou and Makris 2012 (refer to Figure 12 in [27]). Finally, the response of an anchored block to the Rinaldi Station motion closely matched the solution obtained by Makris and Zhang 2001 (refer to Figure 14 in [29]) using two scaling factors for the input ground acceleration, Figure 5.

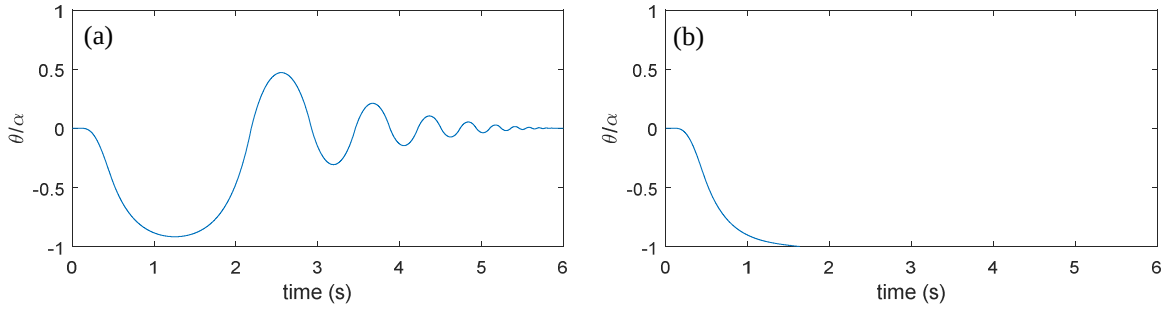

Fig. 3. Rotation time history of a simply supported rigid block (b=0.2m, h=0.6m) subjected to a half-sine pulse (a) no overturning for $PGA = 0.5535g$; (b) right-overturning for $PGA = 0.5545g$.

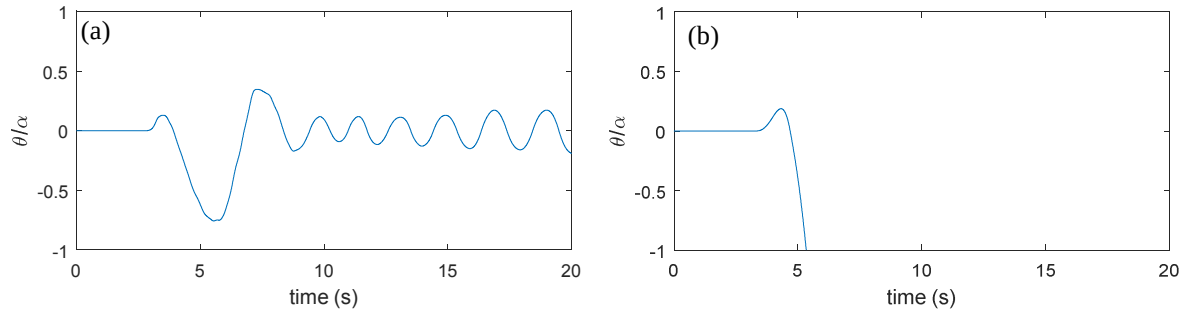

Fig. 4. Rotation time history of a rigid block (b=0.77 m, h=5.17 m) subjected to the Fault-Normal component of the Jensen Filter Plant Motion (PEER RSN983) (a) no overturning of simply supported, and (b) right-overturning of base isolated block ($T_b = 3\ s$, $\xi = 0.1$)

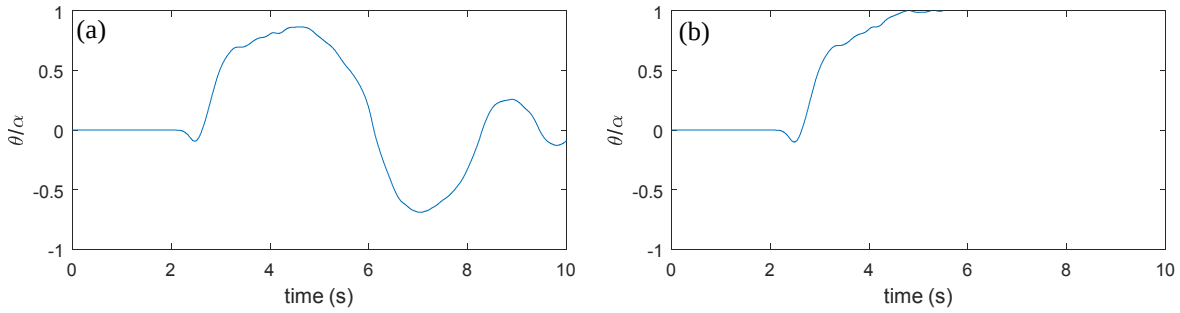

Fig. 5. Rotation time history of an anchored rigid block ($b = 1m$, $h = 3m$, $F_u/W = 0.4$, $\mu = 5$) subjected to the fault-normal Rinaldi Station Motion (PEER RSN1063) (a) no overturning for PGA amplified by 1.18, and (b) left-overturning for PGA amplified by 1.19.

2.2 FRAGILITY FUNCTIONS

Different methods exist for estimating probabilities of failure of rigid blocks subject to ground shaking (e.g., [18, 34]). An incremental dynamic analysis (IDA, [35]) allows the estimation of probabilistic indicators of seismic reliability for given ground motion intensities and collapse fragility curves to any system (e.g., rocking, yielding, flag-shaped). In this study, the electrical equipment was subjected to a set of ground motions scaled to identical peak ground acceleration (PGA) values, and, at each ground shaking intensity, the probability of failure (overturning) is computed as the number of simulations leading to collapse divided by the total number of simulations. The cumulative distribution function (CDF) of the ground shaking intensity y that leads to block overturning is approximately lognormal and can be written as

$$P_F(y) = \Phi\left[\frac{1}{\sigma_{lny}} \ln\left(\frac{y}{\bar{y}}\right)\right] \tag{7}$$

where Φ is the standard normal CDF, $\bar{y}$ is the median value of the distribution (ground motion intensity with a 50% probability of collapse), and σ_{lny} is its standard deviation of $\ln y$.

The fragility functions presented herein use PGA as the ground motion intensity measure (IM), because hazard analyses for PGA are readily available in engineering practice and easier to communicate to decision makers. Nevertheless, the same risk assessment scheme is applicable to other IM's used to predict overturning of rigid blocks, e.g., [36-38], for which ad-hoc fragility functions need to be developed.

2.3 EVALUATION OF SEISMIC RISK

The mean annual rate of equipment failure λ_F is calculated by integrating over all possible y values the probability of equipment failure $P_F(y)$ times the rate of exceedance of the ground motion intensity ([39, 40]) as in

$$\lambda_F = \int_y P_F(y) \left|\frac{d\lambda_y(y)}{dy}\right| dy \tag{8}$$

where $\lambda_y(y)$ is the site-specific seismic hazard curve. The mean annual rate of equipment failure can be conveniently expressed in term of the reliability index β [41] defined as

$$\beta = -\Phi^{-1}(\lambda_F) \quad (9)$$

where $\mathbf{\Phi^{-1}}$ is the inverse of the normal CDF (NORM.INV in Excel).

3. AN ILLUSTRATIVE EXAMPLE

3.1 EQUIPMENT STUDIED

Given the large number of variables involved in this problem, the present study looks at the earthquake toppling risk of nine electrical equipment blocks typically used in Mexican and US power stations [29]. Table 1 presents the equipment mass m and dimensions, and the parameters of the two mitigation measures studied: anchors and base isolation. These equipment represent typical transformers used in substations, covering a wide range of frequency parameters ($1.54 < p < 2.16$ rad/s), and block dimensions ($1.58 < R < 2.49$ m), (e.g., [20, 29]).

For the anchored equipment, the strength (F_u) and yield rotation (θ_y) of the restrainers are specific to each equipment and were also obtained from [29]. A ductility capacity ratio of $\mu = 2$ was defined for all restrainers based on a sensitivity analysis, which showed that larger ductility capacity ratios (e.g., $\mu > 3$ or 4) had only a marginal effect on the reduction of toppling risk, as shown in Figure 6.

For a SCSS base-isolated system, a sensitivity analysis also showed that the fragility functions are not very sensitive to variations of the mass ratio γ between 0.1 and 0.001, and that a stiff base isolation ($T_b = 1\ s$) led to higher β-values in far-field conditions compared to a more flexible interface (e.g., $T_b = 2\ or\ 3\ s$). Henceforth, the SCSS base isolation considered a mass ratio of $\gamma = 0.1$ and a natural period $T_b = 1.0\ s$. The values of the sliding friction coefficient ($\upsilon = 0.05$) and yield displacement ($u_y = 0.25\ mm$) were defined after [27] and were not subjected to parametric variations.

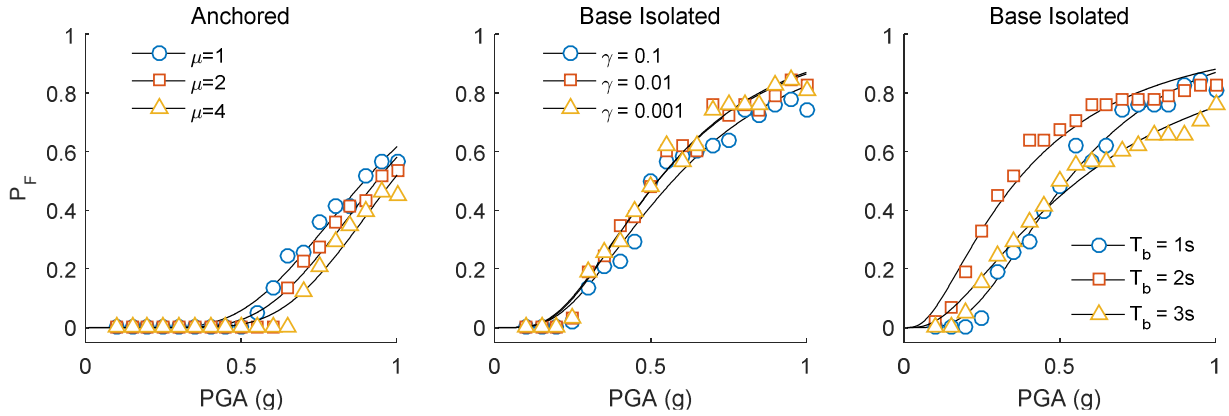

Fig. 6. Fragility functions obtained for equipment EE8 (b=0.88 m, h=2.28 m, W=266.8 kN) subjected to far-field ground motions. Sensitivity analysis for (a) ductility capacity ratio of anchored equipment (F_u/W=0.43, θ_y=7.34×10^{-4}); (b) mass ratio of SCSS base isolation (with T_p fixed at 1s); and (c) base isolation period (with γ fixed at 0.001)

Table 1

Electrical equipment mass and geometric parameters; structural parameters of restrainers and base isolation using a Single Concave Spherical Sliding (SCSS)

Electrical Equipment	Equivalent block dimensions							Anchors *		SCSS Isolation**	
	m	b	h	b/h	α	p	R	F_u/mg	θ_y	m_b	k_b
	kN·s^2/m	m	m	-	deg	rad/s	m	-	rad	kN·s^2/m	kN/m
EE1	18.1	0.91	2.13	0.43	23.2	1.78	2.32	0.100	$3.17\cdot10^{-4}$	$1.63\cdot10^{2}$	$7.16\cdot10^{3}$
EE2	18.1	0.51	1.50	0.34	18.7	2.16	1.58	0.400	$1.33\cdot10^{-3}$	$1.63\cdot10^{2}$	$7.16\cdot10^{3}$
EE3	249.4	1.75	2.54	0.69	34.6	1.54	3.08	0.144	$3.82\cdot10^{-4}$	$2.24\cdot10^{3}$	$9.85\cdot10^{4}$
EE4	87.5	0.97	2.26	0.43	23.1	1.73	2.46	0.275	$6.97\cdot10^{-4}$	$7.88\cdot10^{2}$	$3.45\cdot10^{4}$
EE5	68.0	1.12	1.73	0.65	32.9	1.89	2.06	0.353	$6.02\cdot10^{-4}$	$6.12\cdot10^{2}$	$2.69\cdot10^{4}$
EE6	104.3	0.97	2.29	0.42	22.9	1.72	2.49	0.343	$6.93\cdot10^{-4}$	$9.39\cdot10^{2}$	$4.12\cdot10^{4}$
EE7	79.4	0.97	1.88	0.52	27.2	1.87	2.12	0.451	$6.93\cdot10^{-4}$	$7.14\cdot10^{2}$	$3.13\cdot10^{4}$
EE8	27.2	0.89	2.29	0.39	21.3	1.73	2.46	0.433	$7.43\cdot10^{-4}$	$2.45\cdot10^{2}$	$1.07\cdot10^{4}$
EE9	20.0	0.86	1.73	0.50	26.6	1.95	1.93	0.591	$7.65\cdot10^{-4}$	$1.80\cdot10^{2}$	$7.88\cdot10^{3}$

* *Ductility capacity ratio μ=2, and Bouc-Wen parameters ζ=0.1, $\beta = n = 1$.*

** *Mass ratio $\gamma = 0.1$, , yield displacement $u_y = 0.25$ mm post-yield lateral stiffness $k_b = 4\pi^2(m_b + m)/T_b^2$ with $T_b = 1$ s, sliding friction coefficient $\upsilon = 0.05$, and Bouc-Wen parameters $\zeta = \beta = n = 1$.*

3.2 SEISMIC HAZARD AND GROUND MOTION SELECTION FOR SITES UNDER STUDY

3.2.1 Seismic Hazard

To evaluate the influence of near-source and far-field ground motions, the toppling risk analysis was conducted for the nine equipment hypothetically placed at the sites CALE (near-source) and CU (far-field). Site CALE (18.073°N, 102.755°W) is located on a rock outcrop at the Michoacán Subduction Zone, just 20 km north-west of the epicenter of the great Mw 8.1 Michoacán earthquake of 1985, and has recorded near-source ground motions continuously for over 30 years. Analogously, site CU is located in Mexico City (19.326°N, 99.182°W) over thick deposits of basaltic lava flows at a distance of ~300 km west of the Michoacán Subduction Zone, and 120 km northwest of the 2017 Puebla earthquake, and has recorded far-field ground motions in Mexico since c.1964. Both sites are located on class B sites according to ASCE 7-10 [14].

The ground motion intensity (PGA in this case) and recurrence at each site were computed through a site-specific Probabilistic Seismic Hazard Analysis (PSHA), using the framework developed originally by Esteva-Cornell [42]. Three source types were considered along the Pacific coast of Mexico: subduction interface, intermediate depth intraslab, and shallow crustal faults. According to recent seismic zonation models for Mexico ([43, 44]), these groups were subdivided respectively into 18, 2, and 1 sources, as shown in Figure 7(a). Magnitude recurrence laws within each source were modeled with a truncated exponential distribution, with the exception of three subduction interface sources that follow a Gaussian distribution to account for characteristic earthquakes [45, 46],

The strong ground motions at site CU, located within the hill zone of Mexico City, differ from free-field rock sites on the outskirts of Mexico City. For instance, there is evidence of amplification and de-amplification effects at the hill zone of Mexico City attributed to the local stratigraphy [47, 48]. Therefore, different ground motion models (GMMs) must be used at each

site for more accurate hazard assessment. In this study, the GMMs for subduction earthquakes were obtained from [49] and [50], for the sites CALE (near-source earthquakes) and CU (far-field earthquakes), respectively. Likewise, the ground motions from intermediate-depth intraslab earthquakes were based on the GMMs by [51] (CALE) and [52] (CU), and for shallow crustal earthquakes the GMMs by [53] (CALE) and [54] (CU). The seismic hazard was implemented in the software CRISIS 2014 [55] and the results are shown in Figure 7(b) in terms of the mean annual rate of exceedance of PGA, λ_y. Notice that the PGA hazard at CALE is significantly larger than that of CU. For instance, at λ_y = 0.002 (i.e., 500 year return period), the corresponding PGA is 0.60 g and 0.26 g at sites CALE and CU, respectively. Similarly, at λ_y = 0.0004 (i.e., 2500 year return period) the corresponding PGA is 1.00 g and 0.50 g at sites CALE and CU, respectively.

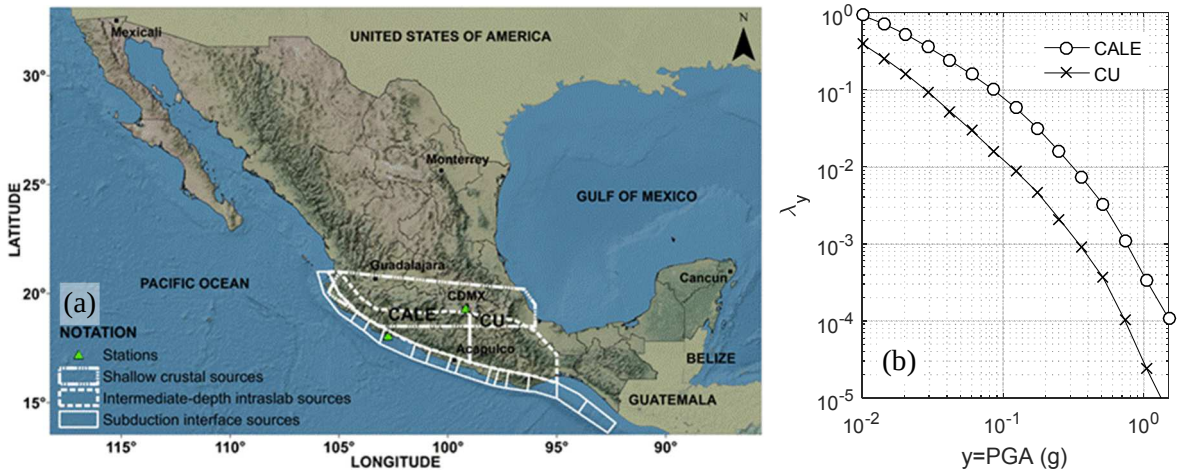

Fig. 7. (a) Mexican seismic sources after [43, 44], and (b) annual rate of exceedance for PGA at station CALE (near-source) and station CU (far-field).

3.2.2 Ground motion selection for incremental dynamic analysis

Since the dynamic response of rigid equipment is highly sensitive to ground motion parameters such as PGA, peak ground velocity (PGV), frequency content, or duration, a careful selection of acceleration records is required. To adequately describe the equipment response and the influence of the input's frequency content, this study used 70 near-source ground motions and 58 far-field ground motions from in 32 Mexican earthquakes recorded between 1964 and 2017. Only ground motions with PGA>0.015 g from earthquakes with magnitudes between 5.9-8.2 were considered. This means that the ground motions required linear scaling factors (SFs) ranging from 1 to 100 to cover the range of intensities needed to establish each fragility function. Further research to assess the consequences of linearly scaling ground motions within the context of an incremental dynamic analysis for rocking bodies is required. Table 2 identifies the earthquake selection and the types of ground motions. Figure 8 shows the location of epicenters (dots) and the stations (triangles), and Figure 9(a) presents the earthquake magnitude and site-to-source distance corresponding to each ground motion used in this study.

353
354
355
356
357 **Table 2**
358 Seismic events used in this study

ID	Date yyyy-mm-dd	Mechanism*	M_w	Hypocenter Location			Number of ground motions **	
				Lat (°)	Lon (°)	Depth (km)	Near-Source	Far-Field
1	1964-07-06	ID-I	7.3	18.03	-100.77	55	-	2
2	1965-08-23	S	7.8	16.28	-96.02	16	-	2
3	1968-08-02	S	7.4	16.25	-98.08	33	-	2
4	1976-06-07	S	6.4	17.45	-100.65	48	-	2
5	1978-03-19	S	6.4	16.85	-99.9	16	-	2
6	1979-03-14	S	7.6	17.46	-101.46	20	-	2
7	1982-06-07	S	6.9	16.35	-98.37	15	-	2
8	1985-09-19	S	8	18.14	-102.71	17	8	2
9	1985-09-21	S	7.6	17.62	-101.82	22	6	2
10	1989-04-25	S	6.9	16.61	-99.43	16	14	2
11	1990-05-31	S	6.1	17.15	-100.85	21	-	2
12	1993-10-24	S	6.6	16.65	-98.87	16	2	-
13	1994-05-23	ID-I	6.2	18.02	-100.57	50	-	2
14	1994-12-10	S	6.6	18.02	-101.56	20	-	2
15	1995-09-14	S	7.3	16.48	-98.76	16	4	2
16	1996-07-15	S	6.6	17.33	-101.21	27	6	2
17	1997-01-11	ID-I	7.1	18.34	-102.58	40	4	2
18	1999-06-15	ID-I	6.9	18.13	-97.54	61	-	2
19	1999-09-30	ID-I	7.4	16.03	-96.96	47	8	2
20	2000-07-21	ID-I	5.9	18.11	-98.97	50	-	2
21	2003-01-22	S	7.5	18.86	-103.90	26	-	2
22	2004-01-01	S	6	17.27	-101.54	17	2	-
23	2007-04-13	ID-I	6	17.09	-100.44	41	2	2
24	2011-12-11	ID-I	6.5	17.89	-99.84	55.3	-	2
25	2012-03-20	S	7.4	16.25	-98.52	16	2	2
26	2012-11-15	ID-I	6.1	18.17	-100.52	40	-	2
27	2013-06-16	ID-I	5.9	18.23	-99.13	52	-	2
28	2013-08-21	S	6.2	16.79	-99.56	20	2	-
29	2014-04-18	S	7.3	17.38	-101.06	16	4	2
30	2014-05-08	S	6.4	17.11	-100.87	17	-	2
31	2017-09-07	ID-I	8.2	14.85	-94.11	58	4	2
32	2017-09-19	ID-I	7.1	18.40	-98.72	57	2	2

* S = *Subduction interface;* ID-I = *Intermediate-Depth Intraslab. ** The symbol "-" denotes non-available record.*

359

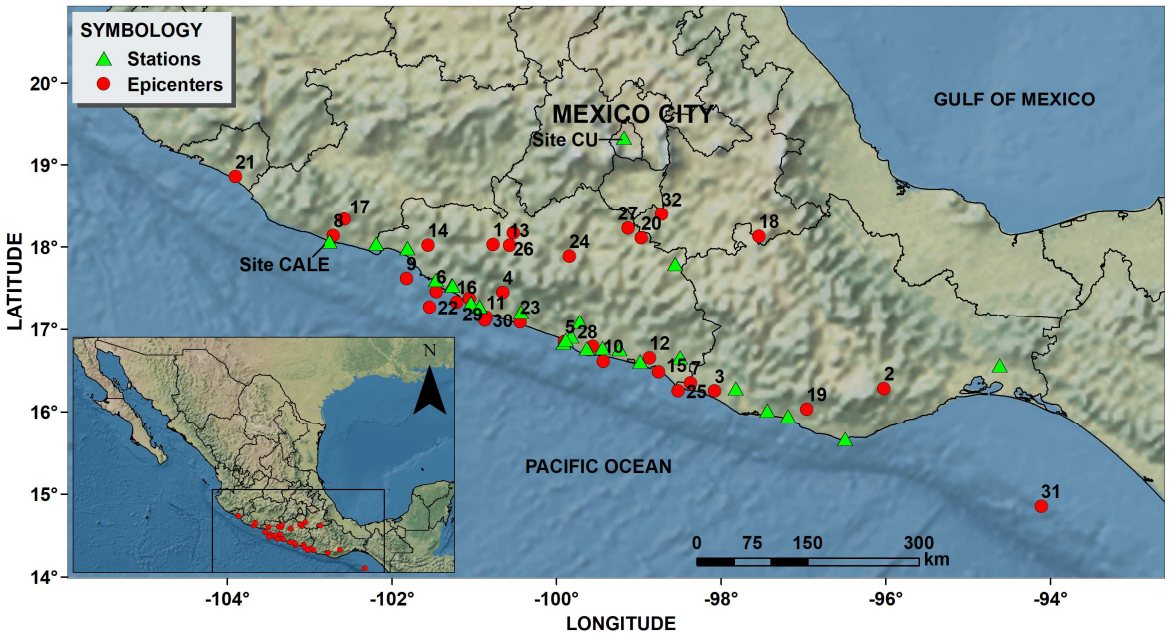

Fig. 8. Epicenters of selected earthquakes and location of ground motion stations.

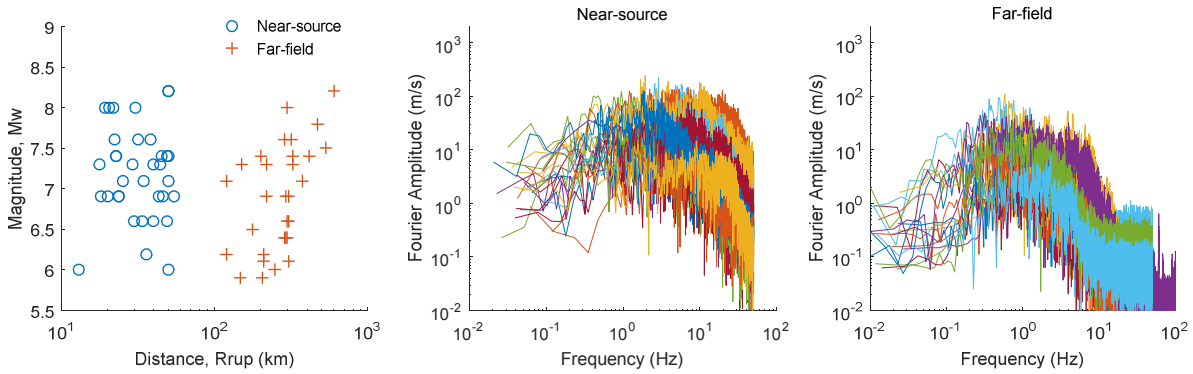

Fig. 9. (a) Magnitude versus site-to-source distance of ground motions used in this study, and Fourier amplitude of (b) near-source acceleration records, and (c) far-field acceleration records.

A close look at the Fourier spectra of the selected acceleration records, Figure 9(b) and Figure 9(c), shows that near-source ground motions deliver most of the energy in the 2-10 Hz range, whereas the far-field ground motions deliver the energy in the 0.2-1.0 Hz range. This aspect is key, as the toppling of small blocks is sensitive to high frequency motions, and the toppling of large blocks is more sensitive to low frequency motions [20]. This study presented herein contributes to the body of knowledge available in terms of the seismic stability of rigid electrical equipment for two bins of ground motions: far field and near field with most of the energy around 0.6 and 6 Hz, respectively. Therefore, further studies for toppling risk assessment of equipment during ground motions with other frequency contents are required.

3.3 SEISMIC RESPONSE OF ELECTRICAL EQUIPMENT

For each support condition (freestanding, anchored, or base isolated), the response of the nine equipment due to the 70 near-source and 58 far-field ground motions was computed numerically. The analysis was conducted for ground motions scaled to PGA between 0.05-1.5

g (near-source) and between 0.05-1.0 g (far-field), in 0.05 g increments, revealing the complex dynamics of single rigid blocks. As an example, details about the seismic response of equipment EE2 (2b=1 m, 2h=3 m) and EE8 (2b=1.8 m and 2h=4.6 m) are presented below for the EW component of the ground motions recorded at stations CALE (near-source) and CU (far-field) during the September 19th earthquake of 1985 Mw 8.1. At each location, the ground motion was scaled to a PGA associated to an annual rate of exceedance of 0.0004, resulting in PGA=1.0g for CALE and PGA=0.5g for CU.

3.3.1 Equipment EE2

Figure 10 presents the response of equipment EE2 for the near-source (CALE) record scaled to PGA of 1.0 g. This figure shows that the simply supported block overturns at t~18 s (left); whereas, the anchored block rocks without toppling and the maximum block rotation is significantly reduced (center). The base-isolated block survives 20 s of ground shaking and its rotation is largely amplified by the base accelerations in excess of 1 g at low frequencies (right). A similar behavior is observed in the EE2 response to the far-field record (Figure 11); even though the ground motion is scaled to PGA of 0.5 g, the long duration and frequency content of the input leads to failure of the simply supported and base-isolated blocks. The restrainers successfully prevent the block from overturning. This example shows that ductile anchors can be an effective mitigation measures against overturning, and that seismic base isolation increases the likelihood of toppling.

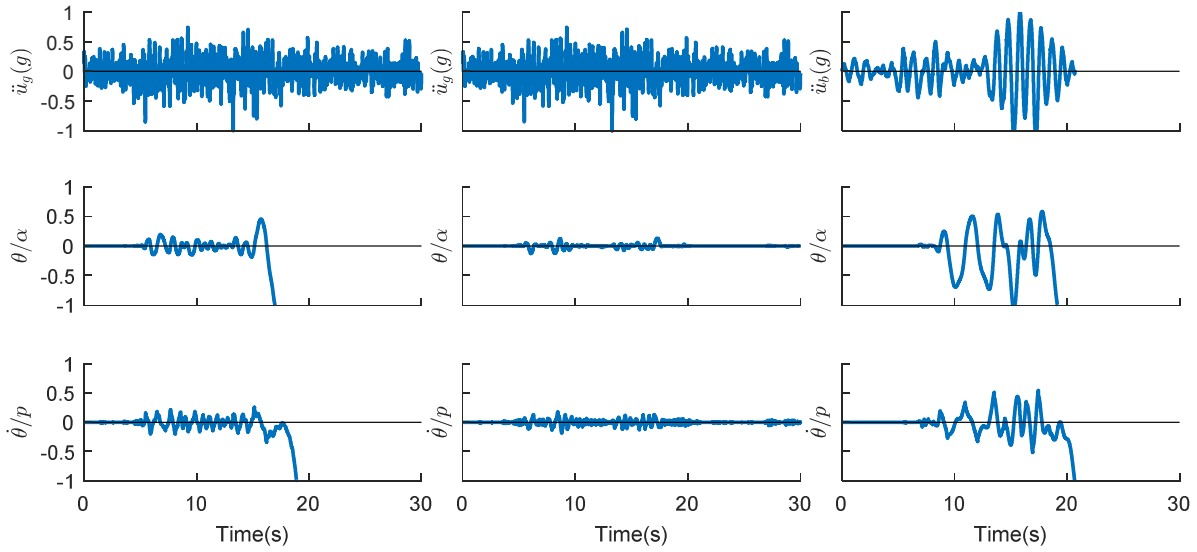

Fig. 10. Seismic response of electrical equipment EE2 to the September 19th 1985 earthquake recorded at CALE station (near-source) scaled to PGA=1.0 g (scale factor of ~2.5). Left: equipment simply supported on a fixed base; center: equipment anchored to a fixed base; right: equipment supported on an isolated base

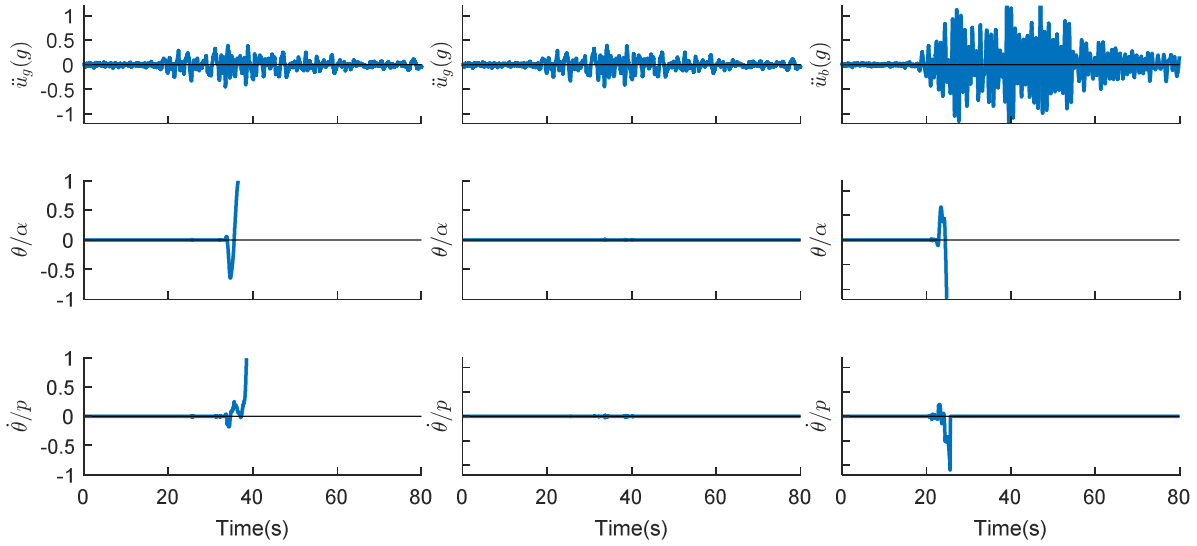

Fig. 11. Seismic response of electrical equipment EE2 to the September 19th 1985 earthquake recorded at CU station (far field) scaled to PGA=0.45 g (scale factor of ~30). Left: equipment simply supported on a fixed base; center: equipment anchored to a fixed base; right: equipment supported on an isolated base

3.3.2 Equipment EE8

Figure 12 presents the response of equipment EE8 subjected to the near-source (CALE) ground motion scaled to PGA of 1.0 g. In this case, the block survives the ground motion for the three support conditions studied, but the base-isolated block (right) undergoes large rotations and low frequency base accelerations; the maximum base displacement relative to the ground is ±25 cm (not shown in Figure 12). The response of EE8 to the far-field record (CU) scaled to PGA of 0.5 g is shown in Figure 13. Contrary to equipment EE2, this much heavier equipment is stable if it stands freely on a fixed base (left); although a very large block rotation occurs at t~40s. The anchored equipment performs very well, and the base isolated equipment overturns at t~28 s, in which case the base isolation is disadvantageous.

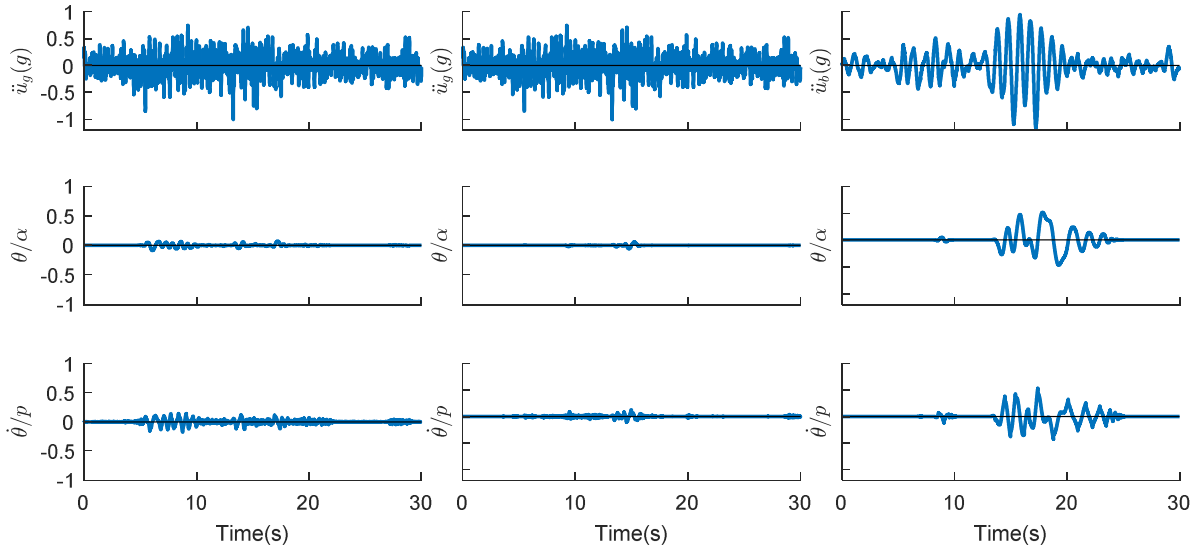

Fig. 12. Seismic response of electrical equipment EE8 to the September 19th 1985 earthquake recorded at CALE station (near-source) scaled to PGA=1.0 g (scale factor of ~2.5). Left: equipment simply

supported on a fixed base; center: equipment anchored to a fixed base; right: equipment supported on an isolated base

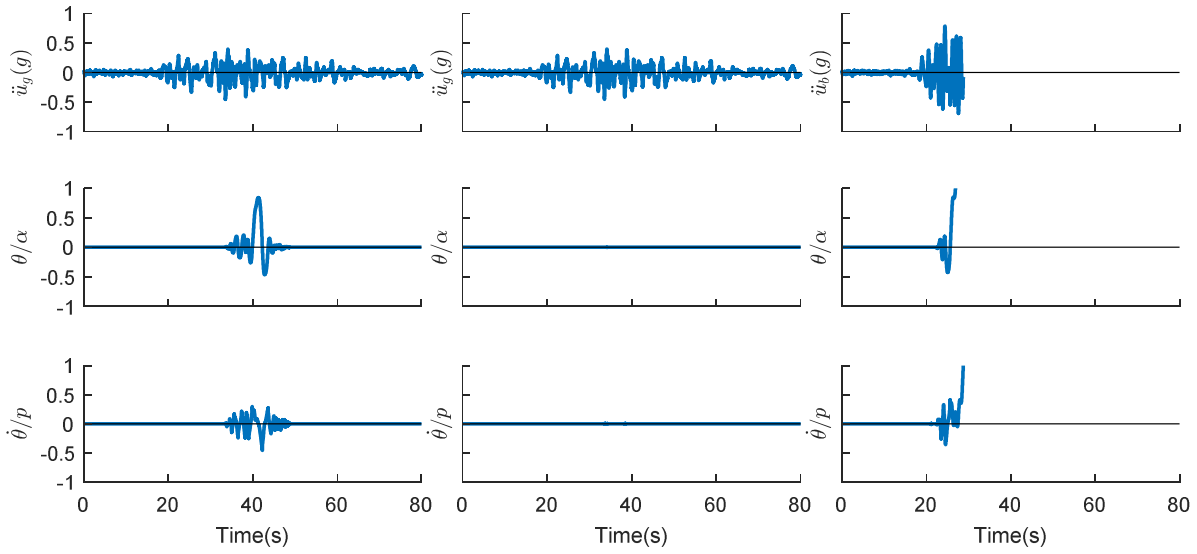

Fig. 13. Seismic response of electrical equipment EE8 to the September 19th 1985 earthquake recorded at CU station (far field) scaled to PGA=0.45 g (scale factor of ~30). Left: equipment simply supported on a fixed base; center: equipment anchored to a fixed base; right: equipment supported on an isolated base

3.4 FRAGILITY CURVES

The failure probability for the nine equipment blocks and the three support conditions was computed numerically and the results approximated with a lognormal distribution as in Eq. (7). This analysis was conducted for the two sets of ground motions, evidencing that the frequency content has a major effect on the block response. As an example, the fragility functions for equipment EE2 (top row), EE8 (middle row), and EE6 (bottom row) are displayed in Figure14. The left and right plots correspond to equipment subjected to near-source (CALE) and far-field (CU) ground motions, respectively. Interestingly, the failure probability for the nine equipment blocks in station CALE is either negligible or very low, with the exception of equipment EE2 supported on a base isolator, which exhibits large failure probabilities for PGA>0.5 g.

In contrast, the probability of failure due to far-field motions increases significantly for all support conditions, the most critical being the equipment simply supported on an isolated base. The use of anchors with a ductility capacity ratio of $\mu = 2$ slightly decreases the failure rates for all equipment studied; further analyses showed that this performance improves slightly with increasing ductility capacity ratios. A careful examination of the fragility functions in far-field conditions shows that the median value of PGA (i.e., PGA associated to a 50% probability of exceedance) increases approximately linearly with the block aspect ratio, b/h, for the three support conditions studied.

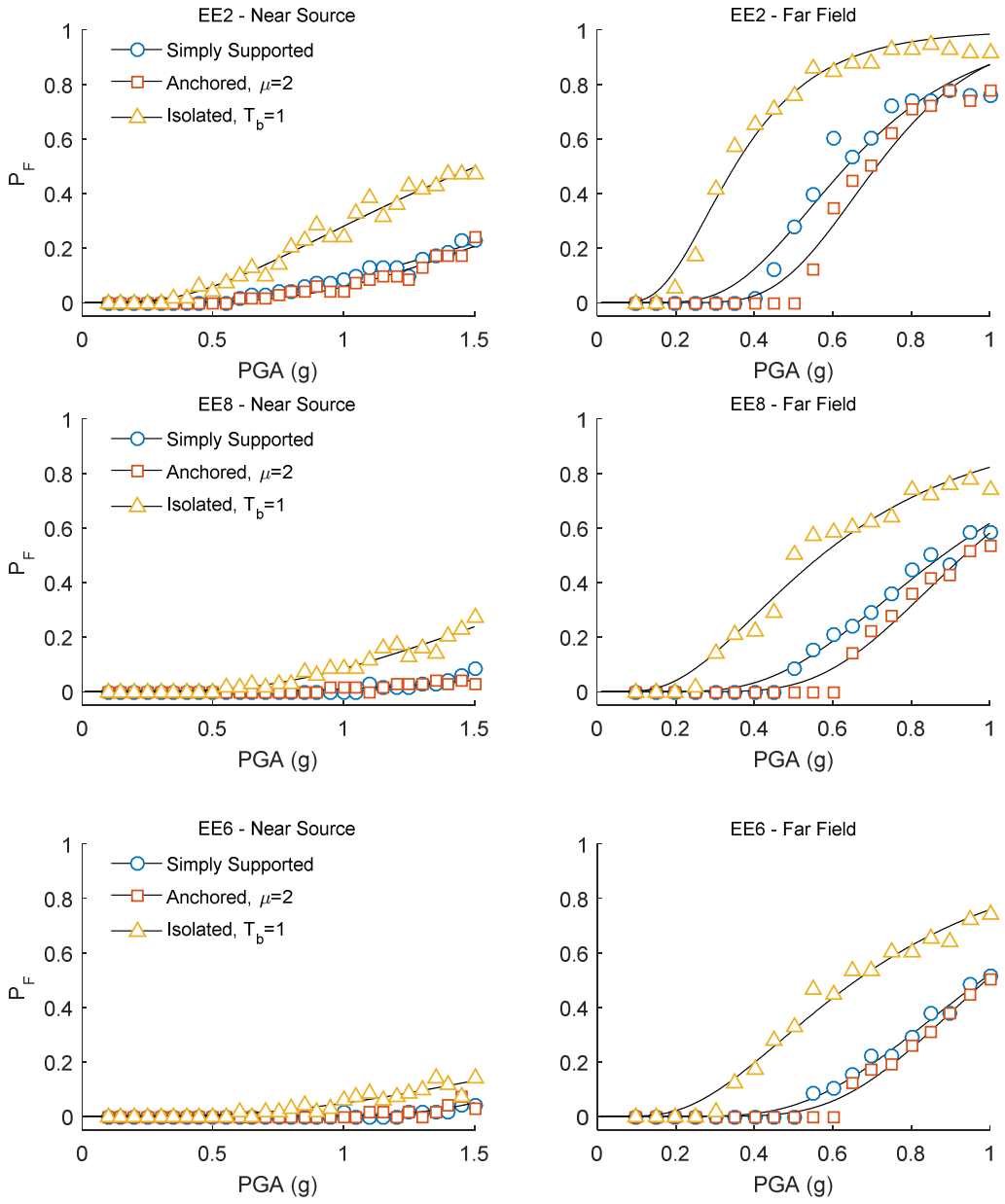

Fig. 14. Fragility functions for equipment EE2, EE8, and EE6 simply supported on a fixed base, anchored to a fixed base, and supported on bilinear base isolator. Results for near-source and far-field ground motions shown on the left and right columns, respectively.

3.5 TOPPLING RISK

The mean annual rate of failure of the equipment was computed by numerically integrating Eq. (8), and expressed in terms of the reliability index β using Eq. (9). The results in Figure 15 show the reliability index versus the block aspect ratio (top) and block size (bottom) for the nine equipment studied. Despite the few toppling events observed in near-source conditions (left plots), it is apparent that the freestanding and anchored equipment have larger β-values than base-isolated equipment. This trend is more evident for equipment in far-field conditions (right plots), as the base-isolated equipment has significantly lower β-values. Overall, the reliability index increase with b/h and R, but this dependence is almost linear with b/h at CU for the three support conditions studied. In fact, for the nine equipment studied, the aspect ratio

is the geometric feature that best correlates with the toppling risk (positive correlation). This results are consistent with observations from past research (e.g., [17, 27, 30]).

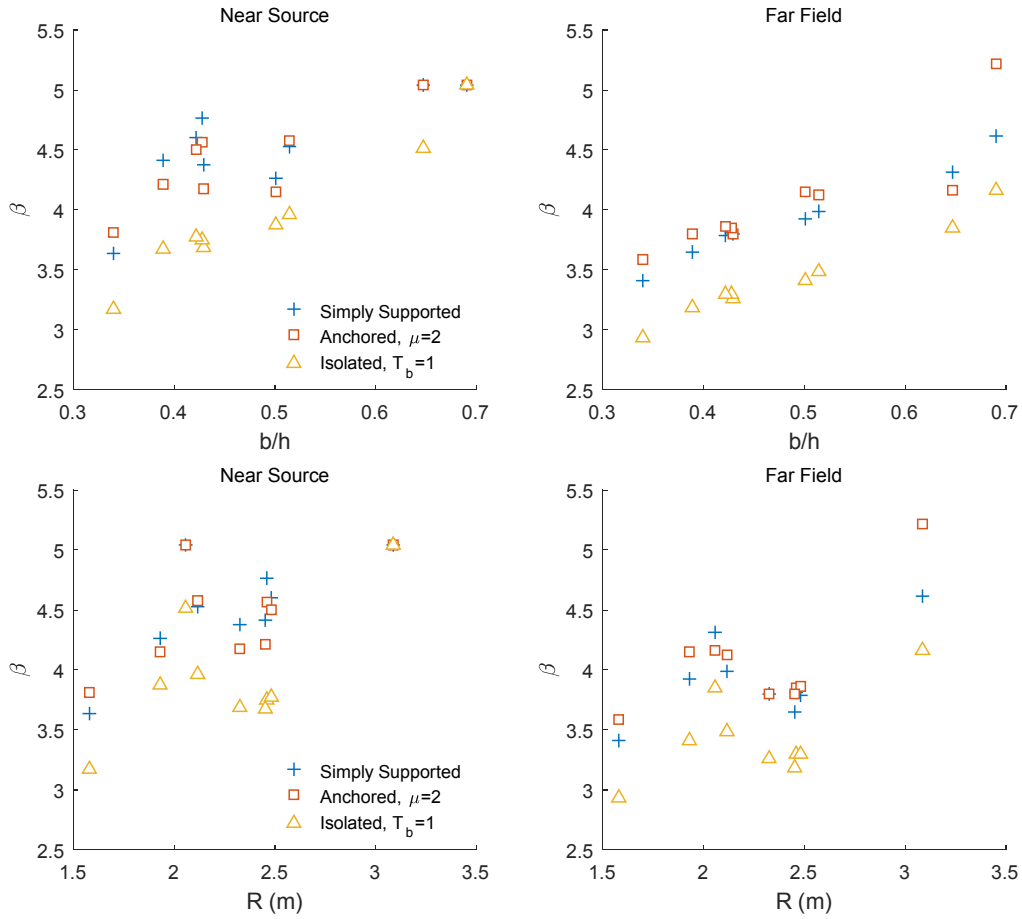

Fig. 15. Reliability index β [41] versus block aspect ratio b/h (top) and block size R (bottom) for equipment under study.

A comparative analysis of the reliability index was conducted for anchored equipment using ductility capacity ratios $\mu = \{1, 2, 4\}$, and base isolated equipment with natural periods $T_b = \{1\ s,\ 2\ s, 3\ s\}$ and a mass ratio of $\gamma = 0.1$. Results are shown in Figure 16 for anchored (top) and base isolated (bottom) equipment. Notice that increasing the anchor ductility improves the response for all equipment, and thus, the toppling risk is reduced. In addition, of the three base isolation periods studied, a period of $T_b = 3\ s$ was more effective in near-field conditions, and a period of $T_b = 1\ s$ was the most effective in far-field conditions.

These integrated results confirm the observations made previously and should aid designers in selecting the proper mitigation strategies against toppling, and identifying the key aspects that influence the response of a rigid electric equipment, e.g., geometry, frequency content of input motion, and support conditions.

CONCLUSIONS

This study evaluates the seismic toppling risk for rigid electrical equipment by integrating their collapse fragility functions and the site-specific seismic hazard. The methodology is implemented for nine equipment used in Mexican and US power plants with height between 3 and 5 m, covering a range of frequency parameters ($1.54 < p < 2.16$ rad/s), and block

dimensions ($1.58 < R < 2.49$ m). Two sets of ground acceleration records from 32 Mexican earthquakes were considered in the development of fragility functions: one set consisting of 70 near-source ground motions and other set consisting of 58 far-field ground motions, which differ primarily in the frequency content and duration. Three equipment configurations were analyzed: 1) equipment simply supported on a fixed base; 2) equipment anchored to the foundations; and 3) equipment supported on an isolated base. The most important conclusions include:

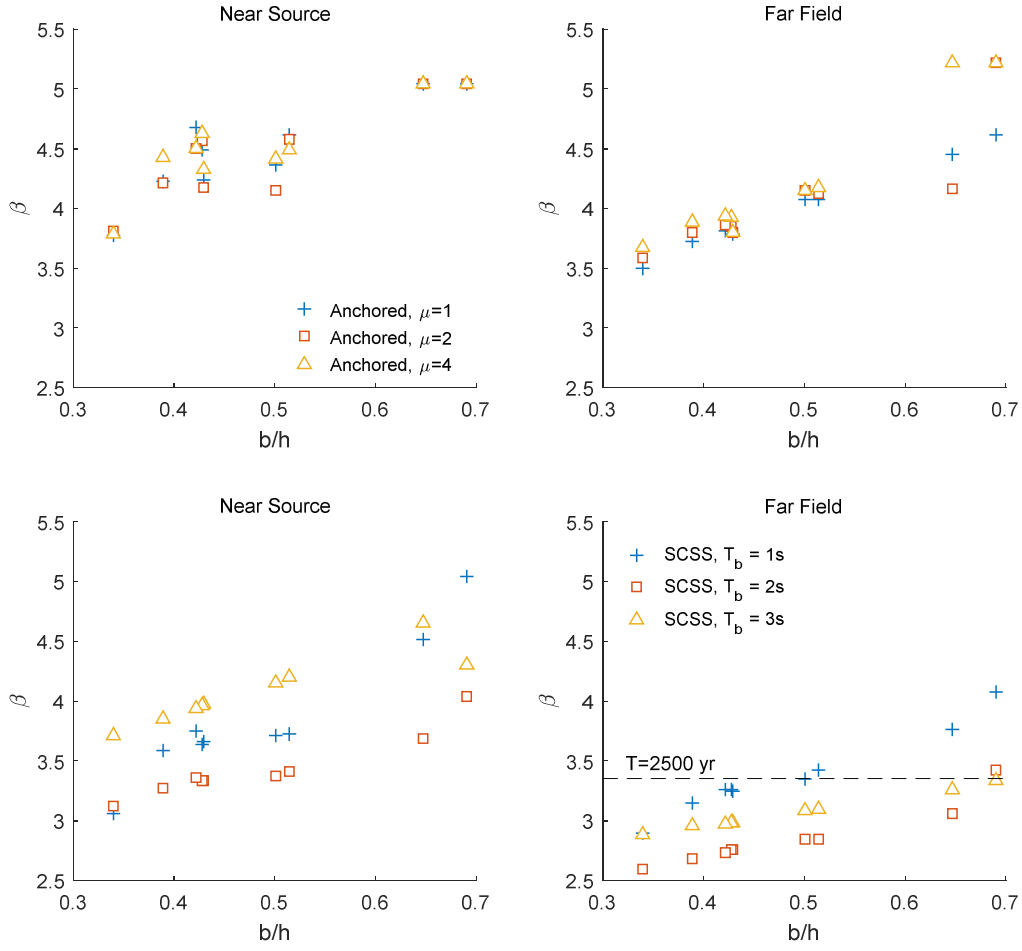

Fig. 16. Reliability index β [41] versus block aspect ratio b/h for anchored equipment (top) and base isolated equipment (bottom) under study.

- For the near-source ground motions, very few collapse events were observed and in most cases, the anchored or base isolated equipment performed just as well as simply supported equipment. With the exemption of the base isolated equipment EE2, the computed reliability indices are above 3.5 (i.e., a return period of 4300 years). Therefore, the implementation of mitigation measures for these conditions may not be justified.

- The set of far-field ground motions caused significantly more collapses than the set of near-source ground motions, because of the lower frequency content and longer duration of shaking. Out of the three configurations analyzed, the anchored equipment was the most reliable (i.e., lower probability of toppling) and resulted in superior

stability compared to the freestanding equipment. Further analysis showed that reliability indices increased slightly with increasing ductility of the restrainers. On the other hand, the use of base isolation with a fundamental period of $T_b = 1s$ was detrimental for all equipment, a condition that worsened with increasing T_b values. This result is consistent with the conclusion by Vassiliou and Makris (2012) [27] about the ineffectiveness of base isolation of large blocks.

- For the two sets of ground motions and the three equipment configurations studied, the reliability index increases almost linearly with the block's aspect ratio, b/h. Likewise, the reliability index increases (not monotonically) with the block size, R. From the results obtained, the aspect ratio is the geometric features that best correlates with the toppling risk of rigid blocks.

Finally, this study presents reference values of the toppling risk for typical electrical equipment subject to strong ground motions and highlights the influence of the ground motions frequency content. These results should aid in the risk assessment of more complex systems and networks; extending this methodology to other seismic environments and equipment is straightforward.

ACKOWLEDGEMENTS

The authors acknowledge the two anonymous reviewers and editor, whose comments and suggestions considerably improved the strength of this article. This research was sponsored by Instituto de Ingeniería at UNAM through the Research Fund for the elaboration of the internal project 6579 "Evaluation of the risk of overturning in rigid electrical equipment during seismic events", Facultad de Ingeniería at Universidad del Desarrollo, the National Research Center for Integrated Natural Disaster Management CONICYT/FONDAP/15110017, and FONDECYT Grant N° 1170836 "SIBER-RISK: SImulation Based Earthquake Risk and Resilience of Interdependent Systems and NetworKs". The authors are grateful for these supports.

REFERENCES

[1] Eguchi R, Seligson H. Lifeline Perspective. Practical Lessons from the Loma Prieta Earthquake 1994;135-163.

[2] Swan S, Conoscente G. Earthquake of October 9, 1995: Effects at the Manzanillo Power Plant. TR-108478, Palo Alto, California. Electric Power Research Institute 1997; pp 3-9, 3-11,3-30 and 3-33. https://nisee.berkeley.edu/elibrary/files/documents/elib/www/documents/201107/EPRI-TR-108478.pdf

[3] Tang AK (Editor). Izmit (Kocaeli), Turkey, Earthquake of August 17, 1999 including Duzce Earthquake of November 12, 1999: Lifeline Performance. Technical council on lifeline earthquake engineering, Monograph 17, ASCE Publications, Virginia USA 2000.

[4] Steinbrugge, K. V. (Photographer) (1971, March 5) Overturned equipment was poorly anchored. Sylmar Converter Station "Intertie" 13201 Sepulveda Blvd. Retrieved from https://nisee.berkeley.edu/elibrary/Image/S4301, The Earthquake Engineering Online Archive NISEE e-Library.

[5] Whittaker, A. (Photographer) (1999, August) Toppled transformer in Enerjisa Transformer Yard. (Izmit, Turkey) Retrieved from https://nisee.berkeley.edu/elibrary/Image/IZT-97, The Earthquake Engineering Online Archive NISEE e-Library.

[6] Bitrán D, Colorado J, García N, Pacheco MA, Reyes C Impacto socioeconómico del sismo ocurrido el 21 de enero de 2003 en el estado de Colima, México, CENAPRED, SEGOB, CEPAL, 2003 (in Spanish).
[7] Rawls C, Turnquist M. Pre-positioning and Dynamic Delivery Planning for Short-term Response following a Natural Disaster. Socio-Economic Planning Sciences, 2012;46(1):46-54.
[8] Arnau O, Chávez M, Guerrero H, Jaimes MA, Pozos A. Observations of damages in some locations of Oaxaca due to the Tehuantepec Mw8.2 earthquake, 6th Structural Engineering World Congress, 2017;14-17 November, Cancun Mexico
[9] PEMEX Petróleos Mexicanos 2017, http://www.pemex.com/en/press_room/press_releases/Paginas/2017-087-national.aspx. Acceded on December 1st, 2017
[10] Jaimes MA, Altamirano P, Reinoso E, López G. Pérdidas en subestaciones eléctricas por sismo. XVII Congreso Nacional de Ingeniería Sísmica, Puebla, Puebla 2009 (in Spanish).
[11] DDF Gobierno del Distrito Federal. Building Code for the Federal District. Official Gazette of the Federal District Government 2004 (in Spanish).
[12] MDOC-DS Manual de Diseño de Obras Civiles-Diseño por Sismo. Comisión Federal de Electricidad 2016 (in Spanish).
[13] NCh2369 National Institute of Normalization. Earthquake-resistant design of industrial structures and facilities (in Spanish). National Institute of Normalization: Santiago, Chile 2003.
[14] ASCE/SEI 7-10. Minimum design loads for buildings and other structures (ASCE/SEI 7-10) 2010.
[15] Bachmann JA, Strand M, Vassiliou MF, Broccardo M, Stojadinović B. Is rocking motion predictable? Earthquake Engineering & Structural Dynamics 2018;47(2):535-552.
[16] Pich P. Nonlinear Rigid Block Dynamics, California Institute of Technology, Pasadena, CA, U.S.A. 1995.
[17] Housner GW. The behavior of the inverted pendulum structures during earthquakes. Bulletin of the Seismological Society of America 1963;53(2):403-417.
[18] Yim CS, Chopra AK, Penzien J. Rocking response of rigid blocks to earthquakes. Earthquake Engineering & Structural Dynamics 1980;8(6):565-587.
[19] Psycharis IN, Jennings PC. Rocking of slender rigid bodies allowed to uplift. Earthquake Engineering & Structural Dynamics 1983;11:57-76.
[20] Makris N, Roussos Y. Rocking response of rigid blocks under near-source ground motions. Geotechnique 2000;50(3):243–262.
[21] Voyagaki E, Psycharis IN, Mylonakis G. Rocking response and overturning criteria for free standing rigid blocks to single—lobe pulses. Soil Dynamics and Earthquake Engineering 2013;46:85-95.
[22] G.P. Cimellaro, M. Chiriatti, B. Qu, in “A New Simple Formula to Evaluate the Risk of Furniture Overturning”, Structures Congress 2014 (American Society of Civil Engineers, Reston, VA, 2014), pp. 1880–1891.
[23] Arredondo C, Jaimes MA, Reinoso E. A simplified model to evaluate the dynamic rocking behavior of irregular free-standing rigid bodies calibrated with experimental shaking-table tests. Journal of Earthquake Engineering 2017;1-26. https://doi.org/10.1080/13632469.2017.1309601
[24] Caliò I, Marletta M. Passive control of the seismic response of art objects. Engineering Structures, 2003;25(8):1009-1018.

[25] Roussis PC, Pavlou EA, Pisiara EC. Base-isolation technology for earthquake protection of art objects. In Proceedings of 14th world conference on earthquake engineering, Beijing, China 2008.
[26] Contento A, Di Egidio A. Investigations into benefits of base isolation for non-symmetric rigid blocks. Earthquake Engineering and Structural Dynamic 2009;8(6):565-587.
[27] Vassiliou MF, Makris N. Analysis of the rocking response of rigid blocks standing free on a seismically isolated base. Earthquake Engineering & Structural Dynamics 2012;41(2):177-196.
[28] Makris N, Zhang J. Rocking response and overturning of anchored equipment under seismic excitations, PEER 1999/06, Pacific Earthquake Engineering Research Center, University of California, Berkeley 1999.
[29] Makris N, Zhang J. Rocking response of anchored blocks under pulse-type motions. Journal of engineering mechanics 2001;127(5):484-493.
[30] Makris N, Black CJ. Uplifting and overturning of equipment anchored to a base foundation. Earthquake spectra 2002;18(4):631-661.
[31] Bouc R. Modèle mathématique d'hystérésis. Acustica 1971;24:16-25.
[32] Wen YK. Method for random vibration of hysteretic systems. Journal of the Engineering Mechanics Division, ASCE 1976;102(EM2):249-263.
[33] Butcher JC. Numerical Methods for Ordinary Differential Equations. John Wiley & Sons 2016.
[34] Reinoso E, Jaimes MA, Esteva L. Seismic vulnerability of an inventory of overturning objects. Journal of Earthquake Engineering 2010;14(7):1008-1021.
[35] Vamvatsikos D, Cornell CA. Incremental dynamic analysis. Earthquake Engineering and Structural Dynamics (2002);31(3):491-514
[36] Kafle B, Lam NT, Gad E F, Wilson J. Displacement controlled rocking behaviour of rigid objects. Earthquake Engineering & Structural Dynamics 2011;40(15):1653-1669.
[37] Gelagoti F, Kourkoulis R, Anastasopoulos I, Gazetas G. Rocking isolation of low□rise frame structures founded on isolated footings. Earthquake Engineering & Structural Dynamics, (2012);41(7):1177-1197.
[38] Dimitrakopoulos EG, Paraskeva TS. Dimensionless fragility curves for rocking response to near-fault excitations. Earthquake Engineering & Structural Dynamics 2015;44(12):2015-2033.
[39] Esteva L. Criterios para la construcción de espectros para diseño sísmico. In 3er Simposio Panamericano de Estructuras, Caracas, Venezuela 1967 (in Spanish).
[40] Cornell CA. Engineering seismic risk analysis. Bulletin of the seismological society of America 1968;58(5):1583-1606.
[41] Cornell CA. A probability-based structural code. In Journal Proceedings 1969;66(12)12:974-985.
[42] McGuire R. Probabilistic seismic hazard analysis: early history. Earthquake Engineering & structural Dynamics 2008;37(3):329-338.
[43] Ordaz M, Reyes C. Earthquake hazard in Mexico City: Observations versus computations. Bulletin of the Seismological Society of America 1999;89(5):1379-1383.
[44] Jaimes MA, Reinoso E. Comparación del comportamiento de edificios en el valle de México ante sismos de subducción y de falla normal. Revista de Ingeniería Sísmica 2006;75:1-22 (in Spanish).
[45] Singh SK, Rodriguez M, Esteva L. Statistics of small earthquakes and frequency of occurrence of large earthquakes along the Mexican subduction zone. Bulletin of the Seismological Society of America 1983;73(6A):1779-1796.

[46] Wesnousky SG. The Gutenberg-Richter or characteristic earthquake distribution, which is it? Bulletin of the Seismological Society of America 1994;84(6):1940-1959.
[47] Ordaz M, Singh SK. Source spectra and spectral attenuation of seismic waves from Mexican earthquakes, and evidence of amplification in the hill zone of Mexico City. Bulletin of the Seismological Society of America, 1992;82(1):24-43.
[48] García D, Singh SK, Herráiz M, Pacheco JF, Ordaz M. Inslab earthquakes of central Mexico: Q, source spectra, and stress drop. Bulletin of the Seismological Society of America 2004;94(3):789-802.
[49] Arroyo D, García D, Ordaz M, Mora MA, Singh SK. Strong ground-motion relations for Mexican interplate earthquakes. Journal of Seismology 2010;14(4):769-785.
[50] Jaimes MA, Reinoso E, Ordaz M. Comparison of methods to predict response spectra at instrumented sites given the magnitude and distance of an earthquake. Journal of earthquake engineering 2006;10(06):887-902.
[51] García D, Singh SK, Herráiz M, Ordaz M, Pacheco JF. Inslab earthquakes of central Mexico: peak ground-motion parameters and response spectra. Bulletin of the Seismological Society of America 2005;95(6):2272-2282.
[52] Jaimes MA, Ramirez-Gaytán A, Reinoso E. Ground-motion prediction model from intermediate-depth intraslab earthquakes at the hill and lake-bed zones of Mexico City. Journal of Earthquake Engineering 2015;19(8):1260-1278.
[53] Abrahamson NA, Silva WJ. Empirical response spectral attenuation relations for shallow crustal earthquakes. Seismological research letters 1997;68(1):94-127.
[54] Jaimes MA, Lermo J, García□Soto AD. Ground□Motion Prediction Model from Local Earthquakes of the Mexico Basin at the Hill Zone of Mexico City. Bulletin of the Seismological Society of America 2016;106(6):2532-2544.
[55] Ordaz M, Martinelli F, Aguilar A, Arboleda J, Meletti C, D'Amico V. CRISIS 2014 V1.2. Program for computing seismic hazard, Instituto de Ingeniería. Universidad Nacional Autónoma de México 2014.

535